Hindawi
Advances in Civil Engineering
Volume 2022, Article ID 9801222, 18 pages
https://doi.org/10.1155/2022/9801222

Research Article

Axial Compression Test and Bearing Capacity Analysis of Biaxial Prestressed Angle Steel Plate Fully Wrapped Reinforced Concrete Short Column

Zhenhua Ren, Xiantao Zeng, Yaqian Shen, and Huanlin Huang

Hunan Key Laboratory for Intelligent Disaster Prevention-Mitigation and Ecological Restoration in Civil Engineering, Hunan Institute of Engineering, Xiangtan 411104, China

Correspondence should be addressed to Xiantao Zeng; xtzeng63@163.com

Received 4 November 2021; Accepted 14 March 2022; Published 9 April 2022

Academic Editor: Wenjie Ge

A new external reinforcement method is proposed in this research by using the prestressed angle steel plate to fully wrap a reinforced concrete column with a rectangular cross section. To study the axial compression characteristics of the new proposed structure, twenty pieces of the concrete columns were built using the normal reinforcement: five control columns and fifteen reinforced concrete columns, with three groups of different prestressed angle steel plates. These columns were tested under axial compression after the completion of the reinforcement. The experimental results showed that the ultimate load-bearing capacities of the three groups of the reinforced concrete columns with different prestress levels were increased by 35.6%, 52.7%, and 61.7% compared with the control columns. Both the ultimate strain and the deformation were improved significantly. The load-bearing capacity equation of the reinforced column was deduced based on the unified strength theory, and the accuracy of the equation was validated. Moreover, a finite element simulation was performed for the new structure, and the simulation results were in good agreement with the test results. Simulation results are in good agreement with the experimental results.

1. Introduction

The most direct method of concrete column reinforcement is transverse reinforcement and axial reinforcement of concrete column; the transverse reinforcement increases the cross section area of concrete, and the stress lag phenomenon exists in the material after addition. Axial reinforcement also increases the transverse dimensions of concrete columns. The prestressed strip reinforcement method can overcome the stress and strain lag and enhance the reinforcement effect; the concrete column is strengthened by applying prestress to the transverse constraint, which makes the concrete in the active three-way compression state, gives full play to its bearing capacity, and then improves the bearing capacity and deformation performance of the concrete column; however, the poor force transmission performance at the joint surface will lead to the poor force of the whole specimen.

Similar to the prestressed strip method, the reinforcement method of using a prestressed angle steel plate for a concrete column with a rectangular cross section was invented by Ren et al. [1]. They conducted a theoretical analysis on the load-bearing capacity of a reinforced concrete column to obtain the calculation formula for short columns. It is well known that a circular concrete column covered with a steel tube has the advantages of high bearing capacity, good seismic performance, light structural weight, and great convenience for construction [2]. A reinforced concrete column using a prestressed angle steel plate has all the advantages of a concrete column covered by a steel tube. Therefore, the research on the axial compression performance of a steel-tube concrete column is the prerequisite for understanding the performance of an angle steel plate's concrete column. Liang et al. [3] analyzed the ultimate bearing capacity of a steel tube by using thick-wall cylinder theory and double-shear unified strength theory, and they

analyzed the load-bearing capacity of a concrete column by using the Drucker-Prager yield theory with the constraint of a steel tube. Their analysis focused on the axially loaded condition of a short concrete column, and they considered the contribution of the vertical stress of a steel tube in a state of yielding to the load-bearing capacity. Their result provided a new method for calculating the ultimate bearing capacity of circular-steel-tube short concrete columns under axial compression. Qin et al. [4] studied the impacts of the concrete strength grade, the steel pipe wall thickness, and the additional amount of steel fiber on the load-carrying performance of short concrete columns. Their research results showed that as the strength grade of the concrete core increased, the ductility of the column deteriorated, and the steel tube could effectively prevent further damage to the concrete core. Moreover, the addition of steel fibers could significantly improve the ultimate strength and the load-bearing capacity in the stationary stage of a steel-tube concrete column. As the steel content in the steel tube increased, the protective constraint effect for the concrete core was enhanced.

Many scholars have investigated reinforced steel-tube concrete columns in recent years. Han et al. [5] conducted experimental research and a theoretical analysis on the axial compression performance of a reinforced steel-tube concrete column. They studied the mechanical behavior, deformation capacity, and failure mode of a short concrete column, and they provided the experimental results for the deformation and ultimate load-bearing capacity, as well as a calculation method for the axial load-bearing capacity. Lu et al. [6] and Gao et al. [7] studied the impacts of various parameters on the load-bearing capacity and ductility of this type of concrete column. They found that different reinforcement methods, the steel tube's wall thickness, and the fly ash replacement ratio had significant impacts on the load-bearing capacity and ductility of the concrete column. Hu [8] carried out axial compression and bias compression failure tests as well as finite element analysis on the load-bearing capacity of a reinforced steel-tube concrete column, and Hu proposed a calculation method for the axial compression load-bearing capacity considering the effect of the initial stress.

The reinforcement method for winding reinforced polymer fibers [9–12] has the advantages of high efficiency, high strength, convenient construction, strong corrosion resistance, wide applications, and small impacts on a structure. Ma et al. [13] carried out comparison tests with axial compression for reinforced circular concrete columns that were wrapped by carbon fiber-reinforced polymers (CFRP) for concrete in a strength range of C40 to C60. They found that the CFRP could effectively constrain the concrete column and improve the compressive properties of the concrete. They also proposed a calculation model for the ultimate compressive strength of the axial compression and the peak strain for a CFRP constrained concrete column. Moreover, they developed a stress-strain relationship model to analyze the improvement effect of the CFRP constraint on the axial compression load-bearing capacity of the concrete column. They analyzed the influences of different factors on the energy density for the axial compression failure of the CFRP concrete column. However, because polymer fiber cloth is a type of anisotropic material, its strength and elastic modulus in the fiber direction are much greater than those in the perpendicular direction. Therefore, this material cannot significantly improve the ultimate load-bearing capacity of a reinforced concrete column.

The reinforcement method of using a prestressed steel strip [14–16] can further improve the load-bearing capacity and deformation performance of a concrete column. Zhang et al. [17] conducted experiments on the mechanical properties of this type of concrete column and found that the failure mode of this type of column was basically the same as that of an unreinforced specimen, while the load for generating the initial crack was higher for the reinforced specimen. Additionally, the prestressed steel strip could significantly enhance the axial stiffness of the reinforced specimen during compression and greatly improve the deformation resistance capability during biased compression.

The rectangular reinforced concrete column with the prestressed angle steel plate is a new product invented by the authors. Its cross section is shown in Figure 1. It is composed of four pieces of angle steel plates that can essentially wrap an entire concrete column. The four sides of each angle steel plate are provided with flanges. The circumferential prestress is applied to the concrete column via the axial flange bolts on the angle steel plate to make the four steel plates and the concrete column into a new structure similar to the steel-tube concrete column. The circumferential constraints given by the angle steel plates can improve the load-bearing capacity of the concrete column. This new reinforcement method has been granted a national invention patent in China (patent no. ZL201610919619.1). The structure is novel in design, and there has been no published research on its performance.

2. Materials and Methods

2.1. Materials and Specimen Design. The design strength grade of the concrete used in the test was C30. According to the *Standard for Test Method of Mechanical Properties on Ordinary Concrete* (GB/T50081-2016) [18], the same batch of the concrete as the rectangular column specimens was selected to conduct the compressive property test. The average compressive strength of the concrete was 30.75 MPa.

The concrete column had a square cross section with a side length of 220 mm and a height of 1000 mm. It was a short column with a slenderness ratio of 4.5, as shown in Figure 2(a). A total of twenty columns were designed for the test, among which five control columns were denoted as CC, and the remaining fifteen columns were divided into three groups of concrete columns having different prestress levels, denoted as RC0, RC2, and RC3.

As shown in Figure 2(b), the material 8Φ12HRBE400E was used for longitudinal reinforcement. According to the *Test Methods of Steel for Reinforcement of Concrete* (GB/T28900-2012), the yield strength of the longitudinal reinforcement was 380 MPa. The material Φ6HPB300 was used for the stirrup with spacing $s = 65$ mm. The yield strength of the stirrup was 275 MPa.

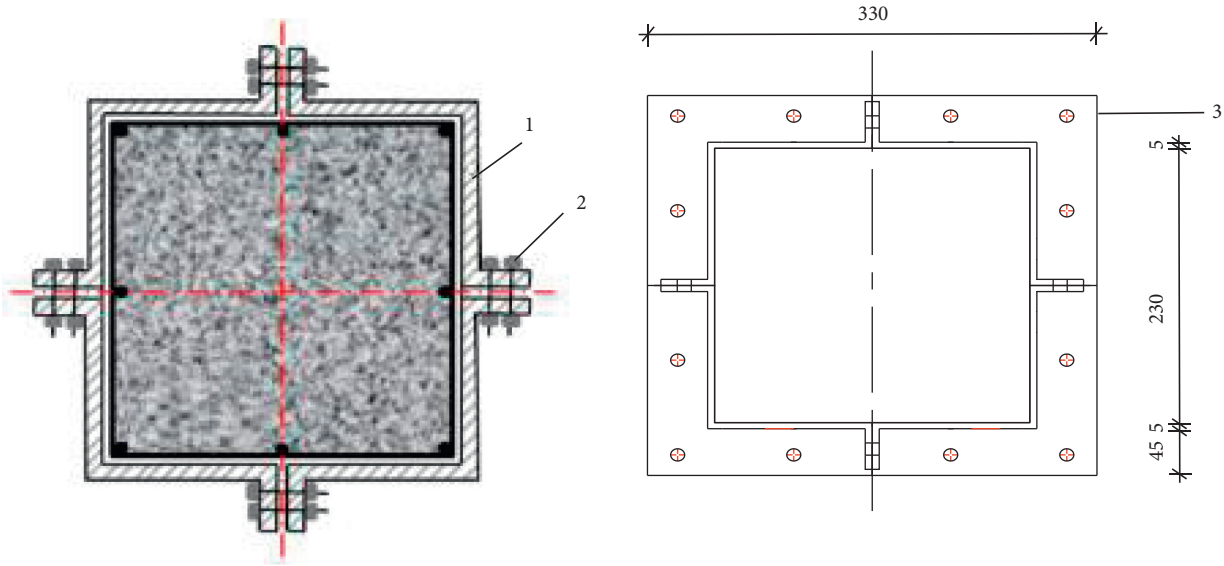

Figure 1: Schematic diagram of reinforcement method.

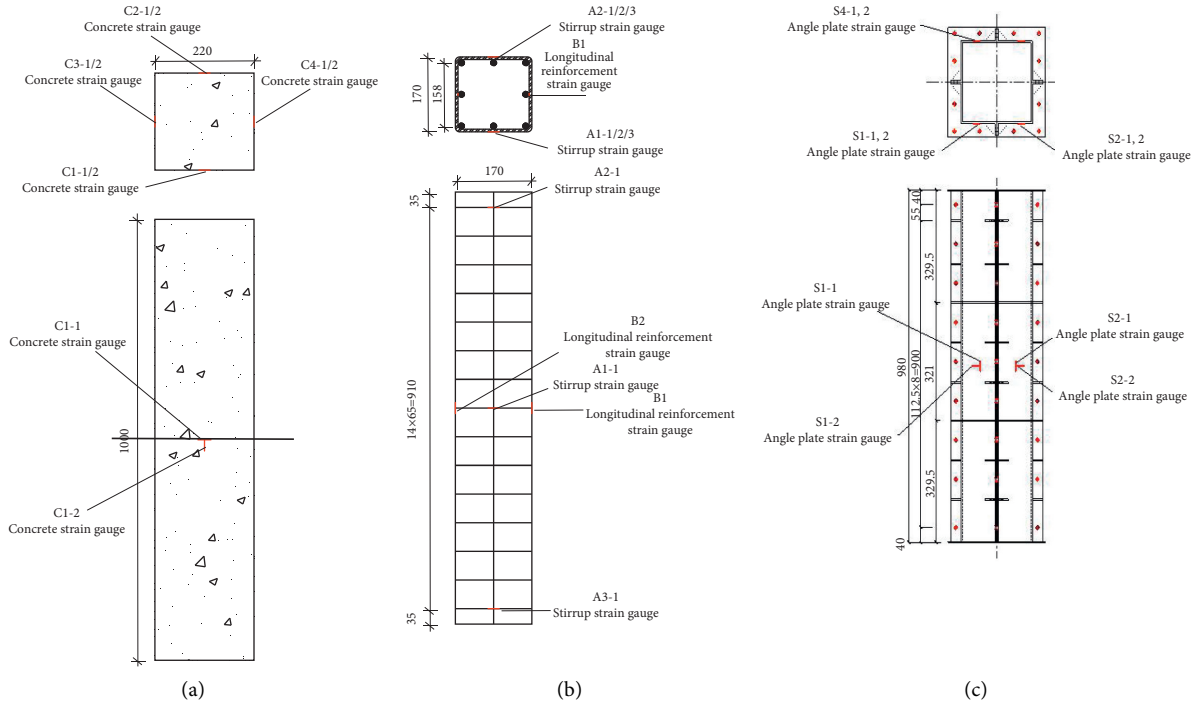

Figure 2: Details of specimens. (a) Concrete. (b) Steel bar. (c) Angle steel plate.

As shown in Figure 2(c), the steel type of the angle steel plate was Q235, the length was 980 mm, and the steel plate thickness was 5 mm. Each single column was strengthened by four pieces of angle steel plates. The four sides of each angle steel plate had flanges and bolt holes. The bolts used in the connections were 8.8 Grade M12 with a diameter of 12 mm. Nine bolts were arranged longitudinally at the joint of the angle steel plate's flange, and a total of 36 bolts were required for each concrete column. To ensure that the circumferential prestress was exerted by the angle steel plates to the concrete column, the four plates did not form a complete square cross section after being closed, and a 6 mm gap was reserved between two adjacent plates, as shown in Figure 2.

Four groups of axial compression tests for the short columns reinforced with the prestressed steel plates were carried out, including the following:

(1) Control column tests without reinforcement

(2) Prestressed column tests including the three following schemes

Scheme 1. The steel plate was fastened on the column without the prestress. The bolts were gently tightened with an ordinary wrench to make the steel plate barely stick to the concrete column. This scheme essentially reflected a reinforced concrete column covered by a steel sleeve.

Scheme 2. The confining pressure of the steel plate on the concrete column was the same as that of the stirrup inside the column on the concrete core, as shown in Figure 3; that is, $\sigma_{r1} = \sigma_{r2}$ (σ_{r1} and σ_{r2} are shown in Figures 3(b) and 3(f), where σ_{r1} is the confining pressure of the steel plate on the concrete column). The wall thickness of the steel plate was much less than the side length of the concrete column. The steel plate thickness was $t = 5$ mm. The cross-sectional area of the steel plate wall was $A_{s1} = 4400\,\text{mm}^2$. The column side length was $b0 = 220$ mm. The concrete column's protective layer thickness was 25 mm. The side length of the concrete core (i.e., the spacing within the stirrup) was 158 mm. The concrete core area was $A_{cor} = 24964\,\text{mm}^2$. The cross-sectional area of the concrete column was $A = 48400\,\text{mm}^2$. The converted area of the stirrup was $A_{ss0} = 274.77\,\text{mm}^2$. Therefore, the constraint stress σ_{r2} of the stirrup acting on the concrete core of the column was calculated with [19]

$$\sigma_{r2} = \frac{f_{yv} \cdot A_{ss0}}{2A_{cor}} = \frac{270 \times 274.77}{2 \times 24964} = 1.49\,\frac{\text{N}}{\text{mm}^2}, \quad (1)$$

where f_{yv} is the design value of the stirrup's tensile strength: $f_{yv} = 270$ MPa. When the confining pressure given by the steel plate to the column was equal to the confining pressure given by the stirrup to the concrete core, there was the following relationship:

$$\sigma_{r1} = \sigma_{r2}. \quad (2)$$

The circumferential tensile stress in the steel plate could be calculated as follows:

$$\sigma_\theta = 2\sigma_{r2}\frac{A}{A_{s1}} = 2 \times 1.49 \times \frac{48400}{4400} = 32.78\,\frac{\text{N}}{\text{mm}^2}. \quad (3)$$

Scheme 3. : The prestress was designed to be the same as the design value of the tensile strength of the fastening bolt. The tensile force sustained by the steel plate was greater than that in Scheme 2. It was assumed that the design value of the axial tensile bearing capacity of a single bolt was N_t^b. Then

$$N_t^b = A_{\text{eff}} f_t^b = 84.3 \times 400 = 33270N, \quad (4)$$

where A_{eff} is the cross-sectional area under the stress of a single bolt: $A_{\text{eff}} = 84.3\,\text{mm}^2$. The parameter f_t^b is the designed tensile strength of the bolt: $f_{\text{t}}^b = 400$ MPa. The number of bolts in each row on the steel plate was nine. Therefore,

$$\sigma_\theta = \frac{N_t^b \times 9}{t \cdot l} = \frac{33270 \times 9}{5 \times 980} = 61.11\,\frac{\text{N}}{\text{mm}^2}, \quad (5)$$

where t is the steel plate thickness: $t = 5$ mm; l is the steel plate height: $l = 980$ mm. The grouping of the test specimens and their prestress values are listed in Table 1.

2.2. Specimen Preparation. The specimen procurement is shown in Figure 4. The steel bars were cut, welded, and bent according to the specification requirements. The processed steel bars were welded and bundled with wires. The leveling steel pad was welded. The steel bars were ground. The strain gauges were pasted on the steel bars and numbered. The concrete was stirred and prepared according to the requirement of the mixture ratio. The concrete prototype was fully vibrated and compacted after pouring and underwent standard concrete curing of 28 days. Water was sprayed on the concrete once every hour in the early stage, once every three hours in the middle stage, and once every five hours in the late stage. After the concrete specimens reached the standard curing period, they were treated with experimental preprocessing procedures such as top leveling and attaching concrete strain gauges and then used in the experiment.

2.3. Loading Program. The YAJ-10000 computer-controlled large electrohydraulic servo compression and shear test machine in the Structure Laboratory of the Construction Engineering Test Center at Zhongnan Forestry University was used in the experiment. It was used to carry out the axial compression test for the short rectangular concrete columns reinforced with prestressed steel plates. The strain gauge measurement locations were on the upper, middle, and lower parts of the concrete columns, as well as on the longitudinal steel bars, the stirrups, the concrete surface, and the outer surfaces of the steel plates. On each concrete column, there were two strain gauge measurement locations on each longitudinal steel bar, six locations on the stirrup, and either four locations on the concrete surface of the control column or four locations on the outer surfaces of the steel plates of the reinforced column. There were twelve strain gauge measurement locations in total. The load was applied in the test according to the Standard for *Test Method of Concrete Structures* (GB/T50152-2012). There were three stages in the test:

(i) Preloading stage: The specimen was first placed in the center of the test device to avoid eccentric compression. The preload was set at 10% of the estimated ultimate load level. The purpose of this stage was to check the safety and reliability of the loading device, check for any abnormal functions of the instrument, and adjust the specimen for mechanical alignment and automatic leveling.

(ii) Standard loading stage: The load was applied with a loading rate of 2 kN/s at the seven following steps: 20%, 40%, 60%, 70%, 80%, 90%, and 95% of the predicted ultimate load level. Each step was held for five minutes.

(iii) Destruction stage: After the load reached 95% of the ultimate load level, the load was not added in steps. Instead, the load was added by displacement control with continuous data acquisition. The load was further increased at a rate of 1 kN/s until the specimen was destroyed. When the load reading on the dial of the test machine decreased sharply, the

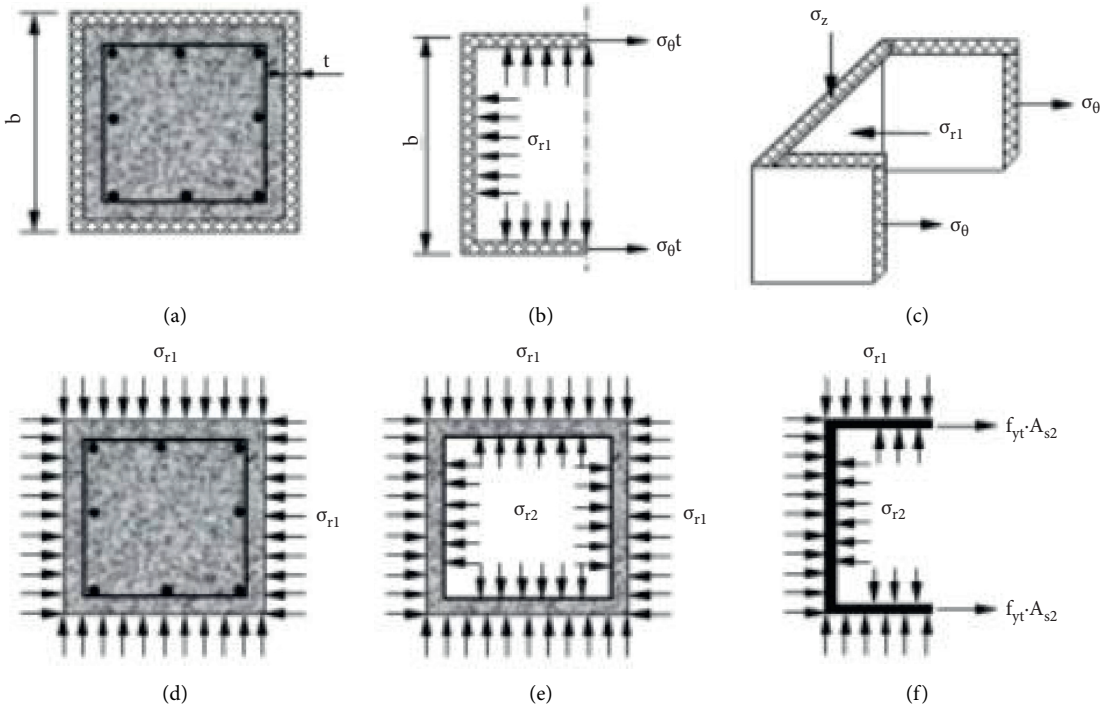

Figure 3: Stress diagram after reinforcement. (a) Column section. (b) Angle plate plane stress. (c) Stereoscopic loading of angle plates. (d) Section overall stress. (e) Protective layer stress. (f) Force of stirrup.

Table 1: Details of specimens.

Methods	Number	Scheme	σ_θ (MPa)	Quantity (pillar)
No reinforcement	RC-1	No angle steel plate	0	5
Reinforcement	RC-2-1	Scheme 1	0	5
	RC-2-2	Scheme 2	32.78	5
	RC-2-3	Scheme 3	61.11	5
Total				20

specimen was close to its ultimate load state and the test was ended. The test loading device is shown in Figure 5.

3. Experimental Results and Phenomena

3.1. Experimental Results. The main test results of the reinforced concrete columns are shown in Table 2. The ultimate load of group RC0 increased by 35.6% on average, and the ultimate load-bearing capacity increased by 43.2% at most. The ultimate load of group RC2 increased by 52.7% on average, and the ultimate load-bearing capacity increased by 56.5% at most. The ultimate load of group RC3 increased by 61.7% on average, and the ultimate load-bearing capacity increased by 73.4% at most. As the prestress increased continuously, the ultimate load-bearing capacity increased significantly. The failure location in the concrete column was mainly concentrated in the middle and lower parts of the column. The steel plates and flanges of groups RC2 and RC3 were deformed and bent, and their bolts began to yield. Because there was a gap between the flanges, the concrete and the steel plate squeezed each other during the axial compression process, resulting in the most serious broken event for the concrete in the gap. Therefore, the concrete in the flange gap was the weak link for compression damage.

3.2. Experimental Phenomena. The concrete column's failure stages in the test included the following: (1) The reinforcement steel bars had yield failures, resulting in a stripping phenomenon between the concrete and the steel bars. (2) The concrete was crushed in a large area, resulting in the bending of the steel plate with the extrusion of the concrete. (3) The concrete completely lost its load-bearing capacity, resulting in deformations in the steel plate's belly and the flange as well as yielding of some bolts.

The control columns were the specimens without reinforcement. In their initial loading stage, the reinforcement steel bars and the concrete were both in the elastic range, and the compressive strain increased uniformly. When the load was increased to approximately 30% of the ultimate load level, subtle longitudinal cracks began to appear at both ends of the column around the corners. When the load was increased to approximately 85% of the ultimate load level,

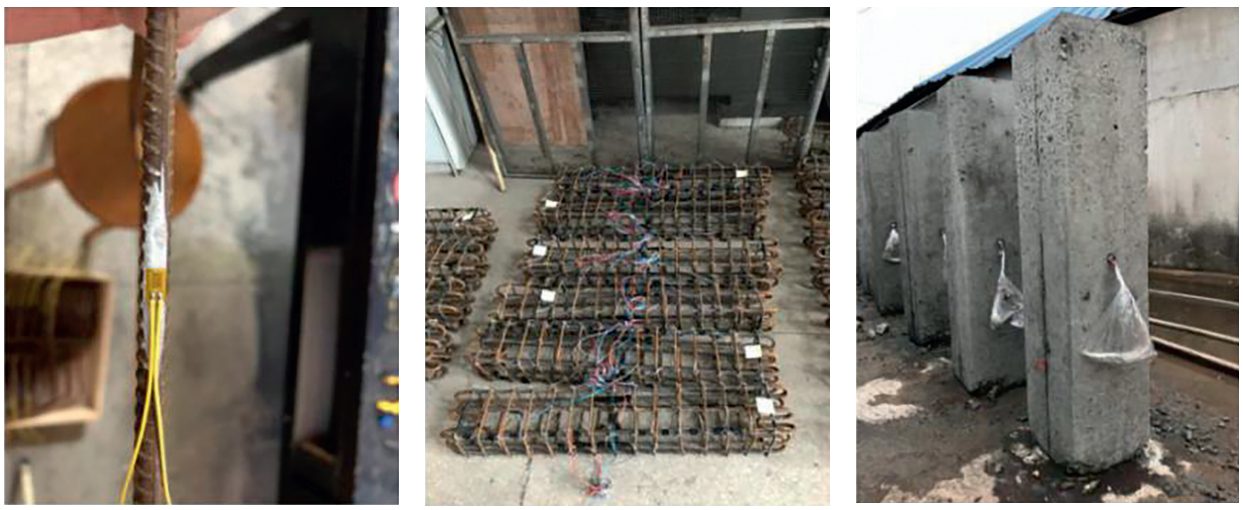

(a) (b) (c)

Figure 4: Process of specimen fabrication. (a) Bonding strain gauges. (b) Reinforcement cage processing. (c) Room temperature maintenance of concrete.

there was an obvious cracking sound and the cracks gradually became wide and extended continuously to the middle. When the load was close to the failure load level, the surface layer of the concrete began to peel off slowly along the cracks, and most of the concrete at the column's corners was crushed. Additionally, the load reading in the dial of the test machine decreased sharply and the specimen was destroyed. These processes are shown in Figure 6(a).

The RC0 column specimens were strengthened by the zero prestress in the steel plates. In the initial loading stage, the concrete column was in the elastic range, and the compressive strain increased uniformly. The load-displacement curve was linear and ascending. The specimen did not have obvious changes in appearance. When the load increased, the concrete column began to have a subtle cracking sound. When the load was increased to approximately 30% of the ultimate load level, the cracking sound was heard everywhere, but the steel plate on the outer surface had no obvious changes.

When the load was increased to approximately 80%, the cracking sound of the concrete core was heard, along with the shooting sound of the cracks when they hit the steel plates. Until the specimen was destroyed, the steel plates did not change significantly, and the upper and lower ends of the reserved compression height of 10 mm were completely pressed. The steel plates were taken off after the load was removed. Obvious cracks were noticed on both sides of the concrete column. When the concrete was struck with a hammer, the concrete in the crushed area immediately peeled off. These processes are shown in Figure 6(b).

The RC2 column specimens were equivalent to the stirrup-reinforced concrete column. In their initial loading stage, the performance of the specimens was similar to that of RC0. When the load was increased to 90%, there were no obvious changes in the steel plates, but the flanges began to be partially stretched and bent. After the load was removed and the steel plates were taken off, it was found that the concrete in the flange gap was seriously damaged. There were obvious and widespread cracks on both sides of the concrete. When the concrete was struck by a rubber hammer, the concrete in the crushed area immediately peeled off. These processes are shown in Figures 6(c) and 6(e).

The RC3 column specimens were designed to have the prestress equal to the design value of the tensile strength of the fastening bolt. In their initial loading stage, the performance of the specimens was similar to that of RC2. When the load was increased to 90%, the steel plate started to have slight bending, and the flanges of the steel plates were seriously strained and bent. Moreover, some bolts reached their yield strength and the damaged bolts jumped out of the screw holes due to the yield fracture. After the load was removed and the steel plates were disassembled, it was found that the concrete in the flange gap was seriously damaged in a powder form. There were obvious and widespread cracks on both sides of the concrete. When the concrete was struck with a hammer, the concrete in the crushed area immediately peeled off. These processes are shown in Figures 6(d) and 6(f).

4. Bearing Capacity Analysis of the New Structure

One control group and three test groups were arranged in the experiment, namely, CC, RC0, RC2, and RC3. The impacts of the prestressed steel plates on the compressive properties of the reinforced concrete columns were studied. According to Table 2, the average test value of each group of specimens was taken. Compared with groups CC, RC0, and RC2, group RC3 increased the load-bearing capacities by 61.7%, 19.2%, and 5.9%, respectively, demonstrating the most significant reinforcement effect. Compared with groups CC and RC0, group RC2 increased the load-bearing capacities by 52.7% and 12.6%, respectively. Compared with group CC, group RC0 increased the load-bearing capacity by

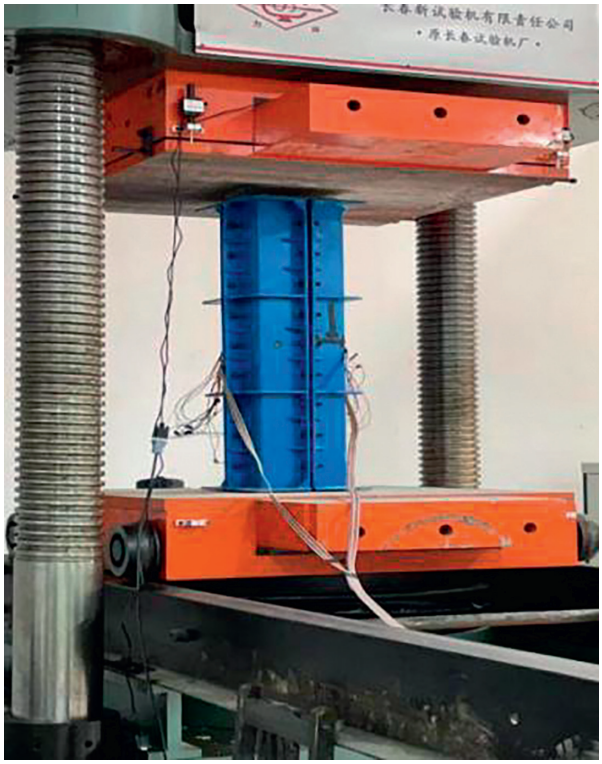

Figure 5: Testing machine.

Table 2: Main results of the test.

Number	N_u(kN)	Increase rate (%)	Failure mode
CC-1	1534	—	Cover concrete spalling, concrete crushing
CC-2	1270	—	
CC-3	1402	—	
CC-4	1445	—	
CC-5	1398	—	
RC0-1	1814	28.7	Steel bar bending, concrete crushing
RC0-2	1853	31.4	
RC0-3	1941	37.7	
RC0-4	1934	37.2	
RC0-5	2019	43.2	
RC2-1	2152	52.6	Axial compression failure of column and deformation of angle plate
RC2-2	2026	43.7	
RC2-3	2181	54.7	
RC2-4	2196	55.8	
RC2-5	2206	56.5	
RC3-1	2444	73.4	Axial compression failure of column, deformation of angle plate and yield of bolt
RC3-2	2443	73.3	
RC3-3	2172	54.1	
RC3-4	2106	49.4	
RC3-5	2233	58.4	

35.6%. The compressive load-bearing capacity of reinforced concrete columns with prestressed steel plates has not been investigated by previous researchers. The authors analyzed the axial compression mechanisms based on their invention patent and the unified strength theory for short column with the longitudinal reinforcement, stirrup, and steel plates. The roles of the steel plate and stirrup in constraining the concrete were studied. A calculation formula for the axial bearing capacity was derived. The calculation results were compared with the test results to validate the formula.

In 1991, Yu established a unified strength theory applicable to different materials based on the double-shear strength theory, using a double-shear element as the mechanics model and considering the influence of the intermediate principal stress. Its mathematical expression is as follows [20]:

Figure 6: Failure modes of typical specimens. (a) CC-2. (b) RC0-1. (c) RC2-2. (d) RC3-1. (e) RC2-2. (f) RC3-1.

$$\left.\begin{aligned} F &= \sigma_1 - \frac{\alpha}{1+\beta}(\beta\sigma_2 + \sigma_3) = \sigma_{ts}\sigma_2 \le \frac{\sigma_1 + \alpha\sigma_3}{1+\alpha} \\ F' &= \frac{1}{1+\beta}(\sigma_1 + \beta\sigma_2) - \alpha\sigma_3 = \sigma_{ts}\sigma_2 \ge \frac{\sigma_1 + \alpha\sigma_3}{1+\alpha} \\ \beta &= \frac{(1+\alpha)\tau_s - \sigma_{ts}}{\sigma_{ts} - \tau_s} = \frac{1+\alpha-B}{B-1} \\ a &= \frac{\sigma_{ts}}{\sigma_{cs}} B = \frac{\sigma_{ts}}{\tau_s} \end{aligned}\right\}, \quad (6)$$

where F, F' is the theoretical function of principal stress intensity. σ_1, σ_2, and σ_3 are the first, second, and third principal stresses, taking tensile stress as positive and compressive stress as negative. σ_{ts}, σ_{cs}, and τ_s are tensile yield strength, compressive yield strength, and shear yield strength of materials, respectively. β is the weighted parameter reflecting the influence of the intermediate shear stress and the corresponding normal stress on the material yield or failure, $0 \le \beta \le 1$. B is the shear stress coefficient.

4.1. Stress Mechanisms. When the concrete column was reinforced by the angle steel plate or the prestressed angle steel plate, the column was similar to the reinforced concrete column with the square steel tube. Its structural process and cross section are shown in Figure 3. It was a column with prestressed confining pressure. The differences between this column and the square-steel-tube concrete column included the following: (1) The four steel plates were prestressed, and the prestress could be adjusted according to the need. (2) The square steel sleeve formed by the four steel plates had no forces in the axial direction of the column. (3) There were gaps in the flange connections of the four steel plates. (4) The concrete column was reinforced by steel bars, and the addition of the four steel plates formed a steel sleeve around the concrete column.

The stress mechanisms of the short concrete column with the steel plates under axial compression were as follows. The concrete core was in a triaxial stress state subject to the constraints of the steel plates and the stirrup. The outer layer of the concrete between the steel plate and the stirrup was constrained by the steel plate and in a triaxial state. The prestressed steel plates were added to the reinforced concrete column. The axial pressure was almost zero. There was tensile stress in the circumferential direction. There was

compression stress (prestress) in the radial direction. The longitudinal steel bars were subject to axial compression.

4.2. Stress in the Angle Steel Plate. As shown in Figure 3, the thickness of the steel plate was t, and the confining pressure of the steel plate on the concrete column was σ_{r1}. The loading condition of the steel plate is shown in Figures 3(b) and 3(c). Because the steel plate could not be pushed too tightly at both ends of the concrete column, the axial compressive stress of the steel plate could be assumed to be. The radial compressive stress was σ_{r1}, and the tensile stress was σ_θ. Then

$$\begin{aligned} \sigma_z &= \frac{N_1}{A_{s1}} = 0, \\ \sigma_{r1} &= -\sigma_r \\ \sigma_\theta &= \frac{\sigma_{r1} b}{2t}, \end{aligned} \tag{7}$$

where N_1 is the axial pressure sustained by the steel plate, which could be approximately zero. As_1 is the cross-sectional area of the steel plate, which was approximately equal to. The parameter is the lateral constraint stress produced by the steel plate on the concrete. The parameter b is twice the width of the steel plate. The parameter t is the wall thickness of the steel plate. The steel plate used for concrete columns is generally very thin, satisfying $b/t \geq 20$, and hence can be regarded as a thin-walled steel pipe, and $|\sigma_r|/\sigma_\theta = (2t/b) \ll 1$, $|\sigma_r| \ll \sigma_\theta$. According to the operating principle of the steel plate, as the concrete strain continuously developed, the circumferential tensile stress σ_θ of the steel plate increased, and the axial compressive stress σ_z gradually decreased. The loading condition of the steel plate changed from mainly sustaining the axial compressive stress to mainly bearing the circumferential tensile stress, and $\sigma_\theta > \sigma_z$. Therefore, the principal stress of the thin-walled steel pipe was

$$\sigma_1 = \sigma_\theta \quad \sigma_2 = \sigma_{r1}\, \sigma_3 = \sigma_z. \tag{8}$$

Substituting the above equation into the discriminant formula of the unified strength theory produced

$$\frac{\sigma_1 + \alpha\sigma_3}{1+\alpha} = \frac{\sigma_\theta + \alpha\sigma_z}{1+\alpha} > 0 > \sigma_2 = \sigma_{r1}. \tag{9}$$

Equation (1) of the unified strength theory was used in combination with Equation (2) and the three principal stresses. The following simplified formula was obtained:

$$\sigma_z = -\frac{1+\beta}{\alpha}\left[\sigma_{ts} - \left(\frac{b}{2t} + \frac{\alpha\beta}{1+\beta}\right)\sigma_{r1}\right]. \tag{10}$$

$$N_1 = \sigma_z A_{s1}. \tag{11}$$

Normally, σ_z is 0, so N_1 is 0.

4.3. Stirrup Stress. The stress conditions of the stirrup and the concrete core in the column are shown in Figure 3(f). When the axial distance between the continuous spiral stirrups or the octagonal stirrups in the compressed column was small, the concrete core could be effectively constrained, and the constrained stress was [21]

$$\sigma_{r2} = \frac{2 f_{yt} \cdot A_{s2}}{s \cdot b_{\text{cor}}}, \tag{12}$$

where σ_{r2} is the constraint stress generated by the stirrup acting on the concrete core, and f_{yt} and A_{s2} are the yield strength and the cross-sectional area of the stirrup, respectively. The parameters s and b_{cor} are the longitudinal spacing and the inner diameter of the stirrup, respectively. Because the force exerted by the steel plate on the stirrup through the protective layer of the concrete was σ_{r1}, the following relationship was obtained from the force balance shown in Figure 3(f):

$$\begin{aligned} (\sigma_{r2} - \sigma_{r1}) &= \frac{2 f_{yt} \cdot A_{s2}}{s \cdot b_{\text{cor}}}, \\ \sigma_{r2} &= \frac{2 f_{yt} A_{s2}}{s \cdot b_{\text{cor}}} + \sigma_{r1}. \end{aligned} \tag{13}$$

4.4. Concrete Load-Bearing Capacity

4.4.1. Before Reinforcement of the Concrete Column. The protective layer of the concrete outside the stirrup was free and only acted as a protective layer. The concrete core in the stirrup was in a triaxial state of stress. The compressive strength of the concrete core could be considered according to the strength of the triaxial compression. Therefore, $f_c' = f_c + 4\sigma_{r2}$, where σ_{r2} is the passive lateral compressive stress (i.e., radial compressive stress) generated by the stirrup on the concrete core. When the stirrup's strain reached the tensile yield strength, the following could be derived:

$$\sigma_{r2} = \frac{f_{yt} \cdot A_{ss0}}{2A_{\text{cor}}}, \tag{14}$$

where A_{cor} is the area of the concrete core counted from the stirrup's inner edge and A_{sso} is the converted area of the stirrup:

$$A_{\text{sso}} = \frac{4 \cdot b_{\text{cor}} \cdot A_{s2}}{s}. \tag{15}$$

4.4.2. After the Concrete Column Reinforced by the Prestressed Steel Plate. The protective layer of the concrete between the steel plate and the stirrup was subjected to the inward force σ_{r1} restrained by the steel plate and to the expansion force (with the same magnitude as σ_{r1}) exerted by the stirrup, as shown in Figure 3(e). The concrete protective layer was equivalent to a stressed cylinder with an inner radius of $b_{\text{cor}}/2$ and an outer radius of $b/2$, subject to an inward stress σ_{r1} and an outward stress σ_{r1}. The stress distribution had to be axisymmetric, and its expression was [22]

$$\sigma_r = \sigma_\theta = \sigma_{r1}. \tag{16}$$

The compressive strength of the outer concrete layer with the triaxial stress, f_{c1}', was

$$f_{c1}' = f_{cy} + k\sigma_{r1}. \tag{17}$$

Then the axial load-bearing capacity of the outer concrete layer, N_2, was

$$N_2 = \left(f_{cy} + k\sigma_{r1}\right)A_{c1} = \left(f_{cy} + k\sigma_{r1}\right)\left[(b)^2 - (b_{\text{cor}})^2\right], \tag{18}$$

where A_{c1} is the cross-sectional area of the outer concrete layer and $A_{c1} = [(b)^2 - (b_{\text{cor}})^2]$. The concrete core was subjected to the dual constraints of the steel plate and the stirrup [23–25] and was in the triaxial stress state. The calculation formula of the axial compressive strength of the concrete for the triaxial stress state was deduced from the unified strength theory in the literature [26] as follows:

$$f_c' = f_{cy} + k\sigma_{r2}. \tag{19}$$

Here, f_c' is the compressive strength of the concrete in the triaxial stress state; $k = (1 + \sin(\phi))(1 - \sin(\phi))$. The parameter ϕ is the internal friction angle of the concrete. k was between 1.0 and 7.0, as determined by testing. When $k = 4.0$, $\phi = 36.87$. The parameter σ_{r2} is the lateral constraint stress of the concrete core, and f_{cy} is the uniaxial compressive strength of the concrete. For the columns with a square cross section, f_{cy} is the uniaxial compressive strength of the prismatic body.

The load-bearing capacity of the concrete core was

$$\begin{aligned} N_3 &= \left(f_{cy} + k\frac{2f_{yt}A_{s2}}{s \cdot b_{\text{cor}}} + k\sigma_{r1}\right)A_{\text{cor}} \\ &= \left(f_{cy} + k\frac{2f_{yt}A_{s2}}{s \cdot b_{\text{cor}}} + k\sigma_{r1}\right)(b_{\text{cor}})^2, \end{aligned} \tag{20}$$

where s is the stirrup spacing and A_{cor} is the cross-sectional area of the concrete core: $A_{\text{cor}} = (b_{\text{cor}})^2$.

4.5. Load-Bearing Capacity of the Longitudinal Reinforcement Steel Bars. When the short reinforced concrete circular column with a steel tube reached the ultimate axial compression bearing capacity, the longitudinal reinforcement steel bars yielded. Therefore, their axial compression bearing capacity N_4 was given by

$$N_4 = f_{ys}A_{s3}, \tag{21}$$

where f_{ys} is the yield strength of the longitudinal reinforcement steel bar and A_{s3} is the cross-sectional area of the reinforcement steel bar.

4.6. Unified Solution of Axial Compression Bearing Capacity. The axial compression bearing capacity N of the short reinforced concrete column with a steel tube was composed of the bearing capacities provided by the steel tube, the outer layer of the concrete, the concrete core, and the longitudinal reinforcement steel bars; that is,

$$N = N_1 + N_2 + N_3 + N_4. \tag{22}$$

After substituting equations (11), (18), (20), and (21) into (22), the unified solution of the axial compression bearing capacity of the short reinforced concrete column with a steel tube was

$$\begin{aligned} N = &-\frac{1+\beta}{\alpha}\sigma_{ts}A_{s1} + f_{cy}\left(A_{c1} + A_{\text{cor}}\right) + k\frac{2f_{yt}A_{s2}}{s \cdot b_{\text{cor}}}A_{\text{cor}} \\ &+ f_{ys}A_{s3} + \left[k\left(A_{c1} + A_{\text{cor}}\right) + \frac{1+\beta}{\alpha}\left(\frac{b}{2t} + \frac{\alpha\beta}{1+\beta}\right)A_{s1}\right]\sigma_{r1}. \end{aligned} \tag{23}$$

When $N_1 = 0$, the equation became

$$\begin{aligned} N = &f_{cy}\left(A_{c1} + A_{\text{cor}}\right) + k\frac{2f_{yt}A_{s2}}{s \cdot b_{\text{cor}}}A_{\text{cor}} \\ &+ f_{ys}A_{s3} + k\left(A_{c1} + A_{\text{cor}}\right)\sigma_{r1}. \end{aligned} \tag{24}$$

The load-bearing capacity was a function of the lateral constraint stress σ_{r1}, because when the circumferential tensile stress of the thin steel plate reached the extreme value $\sigma_{ts} = f_y$, its lateral constraint force also reached the extreme value, and, from $\sigma_\theta = (\sigma_{r1}b/2t) \le \sigma_s = f_y$, the following was obtained:

$$\sigma_{r1} \le \frac{2tf_y}{b}, \tag{25}$$

where f_{y} is the yield strength of the steel plate. Substituting (19) into (18), the maximum axial load-bearing capacity N_{u} was obtained:

$$\begin{aligned} N_u = &-\frac{1+\beta}{\alpha}f_yA_{s1} + f_{cy}\left(A_{c1} + A_{cor}\right) + k\frac{2f_{yt}A_{s2}}{s \cdot b_{cor}}A_{cor} + f_{ys}A_{s3} \\ &+ \left[k\left(A_{c1} + A_{cor}\right) + \frac{1+\beta}{\alpha}\left(\frac{b}{2t} + \frac{\alpha\beta}{1+\beta}\right)A_{s1}\right]\frac{2tf_y}{b}. \end{aligned} \tag{26}$$

When $As_2 = 0$ and $As_3 = 0$, (26) was simplified to the calculation formula of the axial compression bearing capacity of the ordinary short concrete column with a square steel sleeve, given by

$$N_u = -\frac{1+\beta}{\alpha} f_y A_{s1} + f_{cy}\left(A_{c1} + A_{\text{cor}}\right) + \left[k\left(A_{c1} + A_{\text{cor}}\right) + \frac{1+\beta}{\alpha}\left(\frac{b}{2t} + \frac{\alpha\beta}{1+\beta}\right)A_{s1}\right]\frac{2tf_y}{b} = 2b\pi t^2 f_y + \left(f_{cy} + k\frac{2tf_y}{d}\right)A_c. \tag{27}$$

The calculation results obtained using (27) are shown in Table 3.

The load-bearing capacity test results showed that as the prestressed steel plate increased, the load-bearing capacity of the short reinforced concrete column increased significantly. The experimental result was compared with the calculated result given by (27), and the results matched very closely, indicating that the formula could provide guidance for the bearing capacity calculation.

5. Finite Element Analysis of the New Structures

5.1. Finite Element Model Setup

5.1.1. Constitutive Model of the Concrete. The short concrete column reinforced with the steel plate was similar to the steel-tube concrete column in the constitutive model. When the prestress was zero, the columns were equivalent, and the axial compression force of the internal concrete core was a type of passive force that increased with the increase of the vertical axial compression. When the axial compression was small, the concrete column was approximately subject to a unidirectional force. The concrete core did not expand, and the transverse strain was small, with negligible circumferential pressure. When the axial pressure acting on the internal concrete increased, the transverse strain increased and the concrete continued to expand to squeeze the steel plate, producing transverse deformation of the steel plate. The internal concrete was compressed from three directions due to the axial force and the circumferential constraint force.

When the prestress was applied, the steel plate provided an active confining pressure to the concrete core, forming a two-way forcing condition. After the concrete core began to bear the axial pressure, the steel plate produced a lateral constraint effect on the internal concrete column. With the axial pressure exerted by the end of the column, the concrete column was subject to a triaxial state of stress.

Therefore, according to the stress characteristics of the short concrete column, the plastic damage constitutive model suitable for a steel-tube concrete column [27] was used for the new structure in this research. The model was modified based on the unified calculation formula of the stress-strain relationship curve of the axially symmetric triaxial compression of the concrete with different strength grades as follows:

$$y = \begin{cases} \dfrac{A_3 x + (B_3 - 1)x^2}{1 + (A_3 - 2)x + B_3 x^2}, & x \le 1, \\ \dfrac{x}{\alpha_3 (x-1)^2 + x}, & x > 1, \end{cases} \tag{28}$$

where $y = \sigma_{Lc}/f_c^*$, $x = \varepsilon_{Lc}/\varepsilon_f \sigma_{Lc}$ is the axial stress of the concrete, ε_{Lc} is the axial strain of the concrete, f_c^* is the axial ultimate strength of the concrete during the triaxial compression, and ε_f is the axis peak strain of concrete. $f_c^*/f_c = 1 + 3.4\sigma_{Lc}/f_c$, $\varepsilon_f = \varepsilon_c(1 + 3.4\sigma_{Lc}/f_c)[1 + 4.8(A_1 - 1)(\sigma_{Lc}/f_c)^{0.5}]$, $A_3 = A_1[1 + 4.8(A_1 - 1)(\sigma_{Lc}/f_c)^{0.5}]$, and $A_1 = 9.1 f_{cu}^{-4/9}$. B_3 is a physical quantity controlling the attenuation of the elastic modulus of the curve in the rising section. According to the definition of the elastic modulus of the concrete, the rising section was basically a straight line before $\sigma_{Lc} = 0.4 f_c$; that is, when $x = 0.4 f_c^*/A_3$, $y = 0.4 f_c/f_c^*$, B_3 could be obtained as follows:

$$B_3 = \frac{y + (A_3 - 2)xy - (A_3 - x)x}{(1-y)x^2}, \tag{29}$$

where α_3 is the parameter of the descending section of the curve: $\alpha_3 = \alpha_1 = 0.15$. The secant expression of Poisson's ratio of the concrete is expressed as

$$v_c = \begin{cases} v_0, & x \le 1, y \le y_a, \\ v_f - (v_f - v_0)\sqrt{1 - \left(\dfrac{y - y_a}{1 - y_a}\right)^2}, & x \le 1, y_a < y < 1, \\ v_f, & x \ge 1, y < 1, \end{cases} \tag{30}$$

where $v_0 = 0.2, v_0, v_f$ are the initial Poisson's ratio of the concrete and the secant value of Poisson's ratio at failure. According to the analysis of the short concrete columns, $v_f = 1 - 0.0025(f_{cu} - 20)$, $y_a = 0.3 + 0.002(f_{cu} - 20)$ was satisfactory for accurate simulations.

5.1.2. Constitutive Model of Steel. The ideal steel elastic-plastic model was used to model the constitutive relationship of steel. The steel materials in the test included the longitudinal reinforcement steel bar, the stirrup, and the angle steel plate. Due to their similar properties, the constitutive relationship curves of these steel materials were the same.

Table 3: Bearing capacity test results of each group.

Number	N_c (kN)	$\overline{N_t}$ (kN)	Error (%)
CC	1461.38	1409.80	--
RC0	1930.98	1912.04	0.98
RC2	2219.44	2152.22	3.03
RC3	2469.19	2279.91	7.67

Note: N_c and $\overline{N_t}$, respectively, are the calculated value and average test value of specimen bearing capacity.

The relationship was an ideal elastic stage before the steel material reached the yield strength, and the relationship entered the plastic stage after the material reached the yield strength. Its expression is shown as follows:

$$\begin{cases} \sigma_s = E_s\varepsilon_s, & \left(\varepsilon_s \le \varepsilon_y\right), \\ \sigma_s = f_y, & \left(\varepsilon_s > \varepsilon_y\right). \end{cases} \tag{31}$$

The following assumptions were adopted in the finite element simulation:

(1) There was limited slip between the angle steel plate and the concrete.

(2) The stress-strain relationships of steel and concrete were determined according to equation (31).

(3) Only the longitudinal equilibrium and the deformation coordination were considered

5.2. Finite Element Calculation Model

5.2.1. Element Type Selection. `The research object was the internal concrete core. Therefore, the angle steel plate was simplified to an equivalent steel sleeve, and the influence of the high-strength bolt connection was ignored. The shell element (S4) of the fully integrated form of the four nodes was used for the angle steel plate. The three-dimensional solid element (C3D8R) with the reduced integral form of the eight nodes was used for the concrete core. The truss element of T3D2 was used for the reinforcement steel bars.

5.2.2. Model Setup and Mesh Division. Different parts in the finite element model were defined with the constitutive models and the section characteristics according to different material types, including the concrete, the reinforcement steel bar, the angle steel plate, and the upper and lower cushion blocks. The simulation parameters of the concrete column were the same as the parameters used in the test, that is, a rectangular section of 220 mm $\times$ 220 mm, a column height of 1000 mm, a longitudinal length of the reinforcement steel bar of 980 mm, a steel sleeve (equivalent angle steel plate) length of 980 mm, and a stirrup side length of 170 mm. An entity is the mapping object of the component in an assembly. An entity can be independent or dependent. The components were defined as dependent entities, and grid division in the assembly was not possible for the components. Therefore, grid division was conducted for each component separately in this research. According to the finite element computational time, an appropriate mesh density was selected in mesh division. The meshing result is shown in Figure 7.

5.2.3. Section Contact Definition. When the contact surface was defined in the finite element model, the embedded contact between the reinforced skeleton and the concrete was selected without considering the influence of the bond-slip. The interface model between the angle steel plate and the concrete was composed of the normal and tangential bond-slips. The "hard" contact was selected to model the normal contact between the angle steel plate and the concrete core. The coulomb friction model was used to simulate the tangential force transfer. The nested model was used to simulate the interface between the reinforcement steel bar and the concrete, and the steel bar was assumed to be nested into the concrete as a whole. The Tie binding model was selected to simulate the contact surface between the upper or lower pad block and the concrete.

5.2.4. Boundary Condition Definition and Loading Simulation. In the boundary condition definition of the finite element model, it was necessary to define the boundary conditions of the two cushion blocks. A fixed constraint boundary condition was added to the bottom pad of the column. The constraint condition for the upper pad was set to move only along the z-axis.

The experimental test required prestress during the loading process. Therefore, three analysis steps were simulated in the model: Initially we have Step 1 and Step 2. In the initial stage, the constraints were set up on various contact surfaces. The prestress exerted by the high-strength bolts in the test was simplified in the simulation into the circumferential confining pressure exerted on the steel sleeve. Therefore, the circumferential pressure was exerted on the short column in Step 1. The pressure was produced with direct uniform distribution. The axial loading process was simulated in Step 2. The loading method was displacement loading, which was achieved by applying a surface load on the upper pad of the concrete column.

During the loading process in the test, the prestresses were the pretightening forces exerted by the high-strength bolts, which were 0 MPa, 179.5 MPa, and 340 MPa. According to (1) and (5) for the confining pressure of the angle steel plate, the uniform distributed loads exerted on the equivalent side steel sleeve were 0 N/mm^2, 1.49 N/mm^2, and 2.78 N/mm^2.

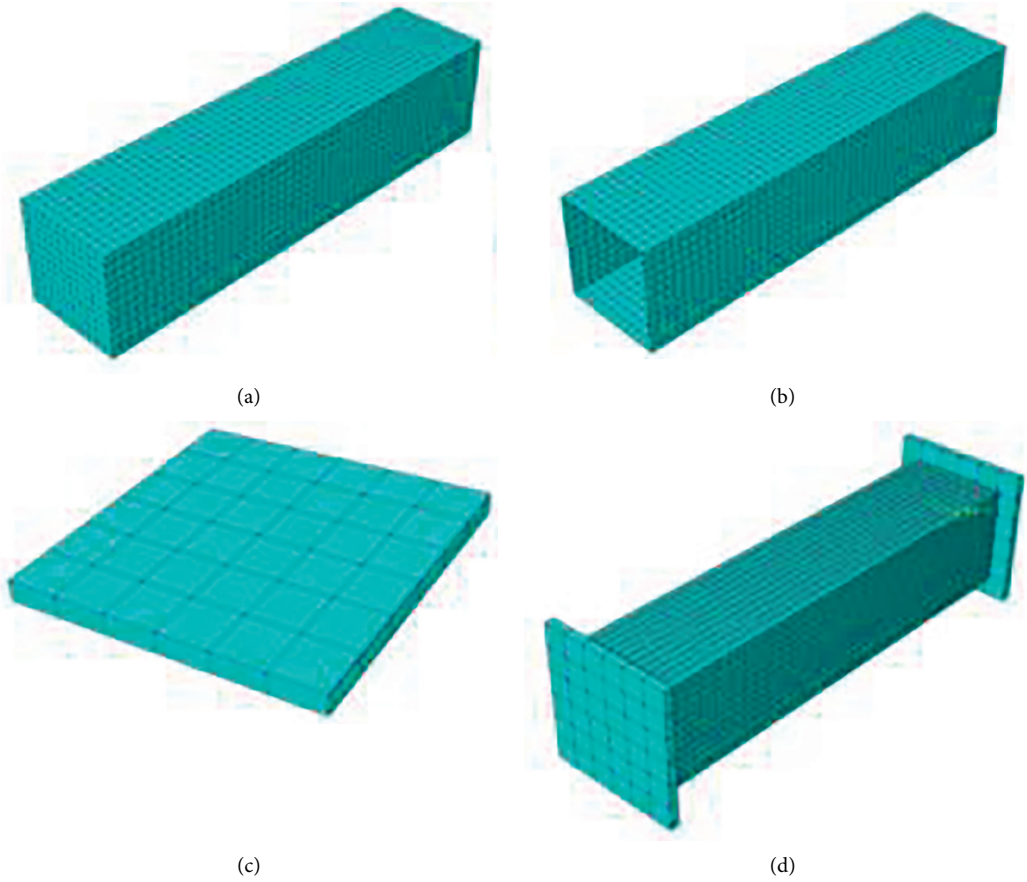

Figure 7: Model mesh subdivision. (a) Concrete. (b) Angle steel plate. (c) Cushion block. (d) Whole model.

5.2.5. Finite Element Solution. After the above operations were completed, the finite element calculation was started. During the simulation, the computational process was monitored by using related functions in ABAQUS. When the software reported an error, the problem was diagnosed according to the system prompt and the model was modified to fix the problem.

5.3. Analysis of Finite Element Simulation Results

5.3.1. Validation of Finite Element Simulation. Table 4 shows that the ultimate bearing capacity of each specimen was obtained through finite element simulation. The simulation data and the test data were very close when compared, with an error within 5%, meeting engineering calculation requirements. N_m in Table 4 is the simulated ultimate load and N_t is the tested ultimate load.

Figure 8 shows the curves of the load versus vertical displacement of the four groups of specimens. With the reinforcement effect of the confining pressure given by the steel plates, when the specimen reached the maximum bearing capacity, the curve retained a slow decline and tended to level off. When the simulation result of this type of curve was compared with the test results for all the groups of specimens, there was a small difference.

5.3.2. Finite Element Analysis Results. In order to further study the stress characteristics of the short concrete column reinforced with the steel plate under axial compression, ABAQUS was used to perform finite element analysis to obtain the stress variations of the steel plate and the stress distribution chart with the ultimate load, as shown in Figure 9.

The stress distribution maps of RC1, RC2, and RC3 were analyzed. The maximum stress was concentrated in the corner of the rectangular angle steel plate. The first location of the buckling deformation was concentrated in the middle and upper regions of the steel plate. Compared with RC2, as the RC3 prestress increased, the coverage range of the maximum stress on the RC3 steel plate increased and was distributed in the middle area of the component.

Figures 10–13 show the plastic PEMAG charts of the CC, RC1, RC2, and RC3 specimens, which recorded the plastic strains of the concrete columns when the bearing capacities reached the failure loads in the deformation process. By comparing the CC columns with reinforced columns, it was found that the plastic strain in the red area of the CC columns in the control group was small, while the plastic strains of the RC1–RC3 columns were increased 1-2-fold, indicating that the proposed reinforcement method could improve the ductility of the concrete columns.

Table 4: Comparison of experimental and calculated values.

Number	f_c (MPa)	Prestress (MPa)	N_m/kN	N_t/kN	N_m/N_t
CC	30.1	—	1413.56	1409.80	1.02
RC1	30.1	0	1955.22	1912.04	1.02
RC2	30.1	179.5	2171.83	2152.22	1.01
RC3	30.1	340	2271,39	2279.91	1.00

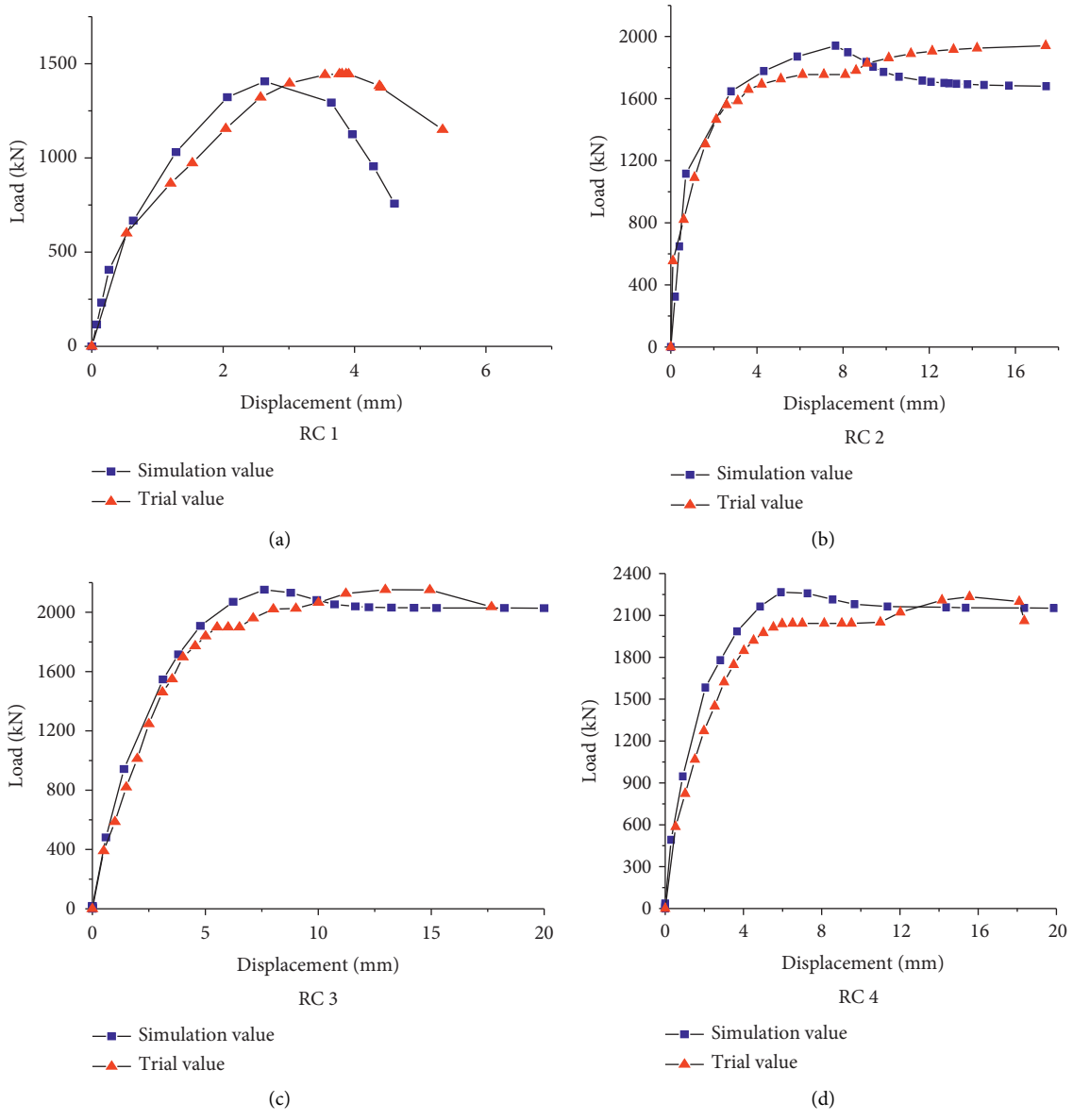

Figure 8: Comparison of load-displacement curves between test and simulation. (a) RC1, (b) RC2, (c) RC3, (d) RC4.

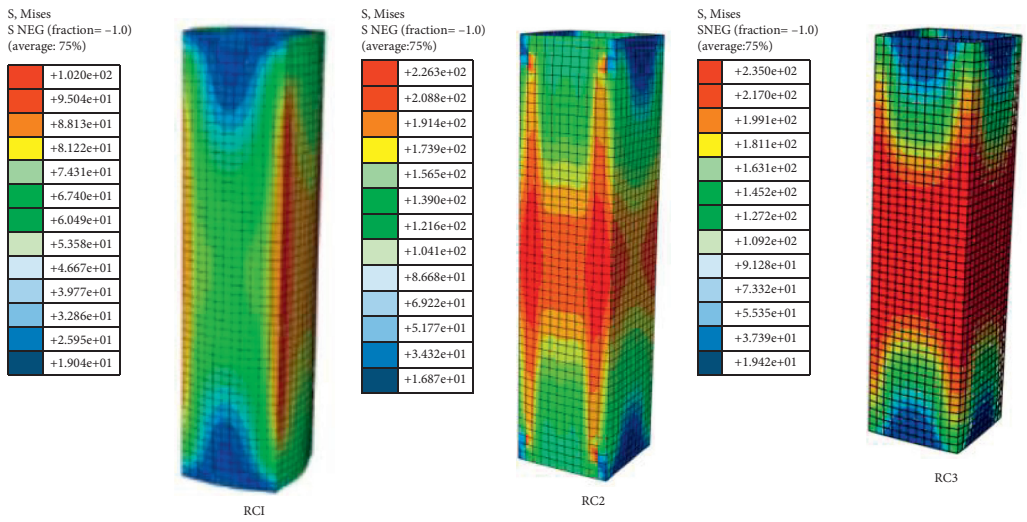

Figure 9: Stress nephogram of angle plate.

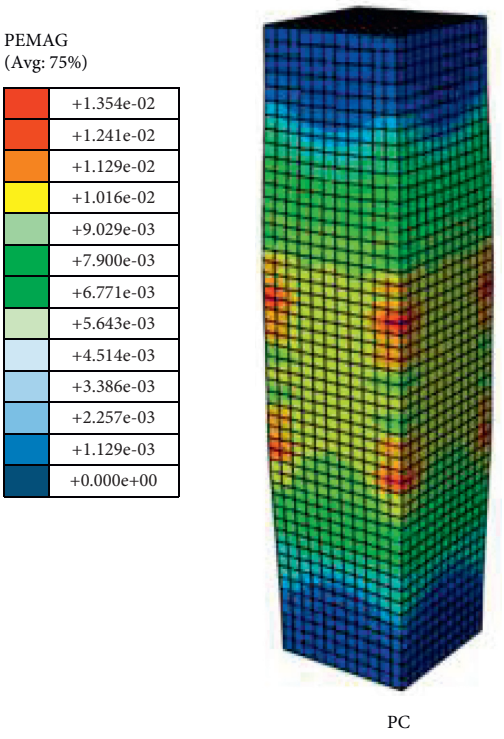

Figure 10: Strain cloud picture of CC (MPa).

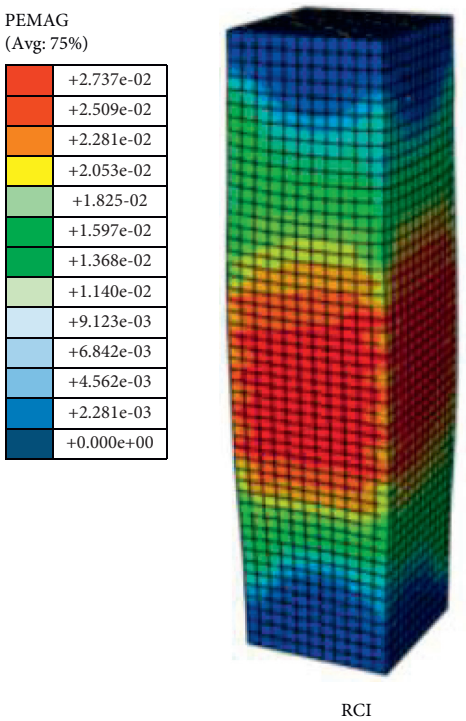

Figure 11: Strain cloud picture of RC1 (MPa).

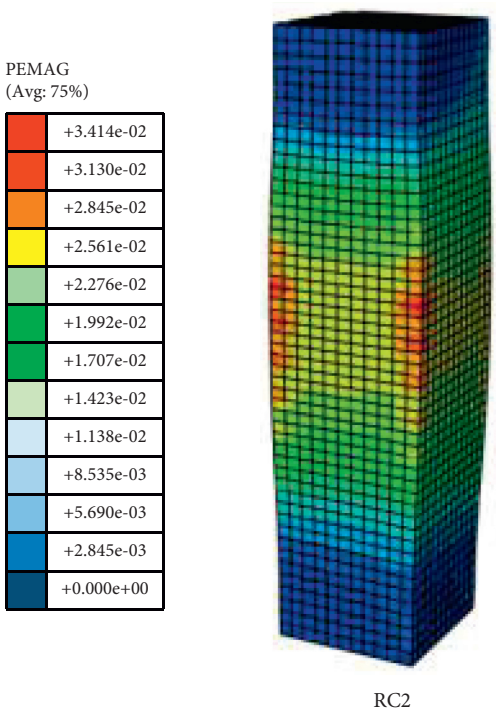

Figure 12: Strain cloud picture of RC2 (MPa).

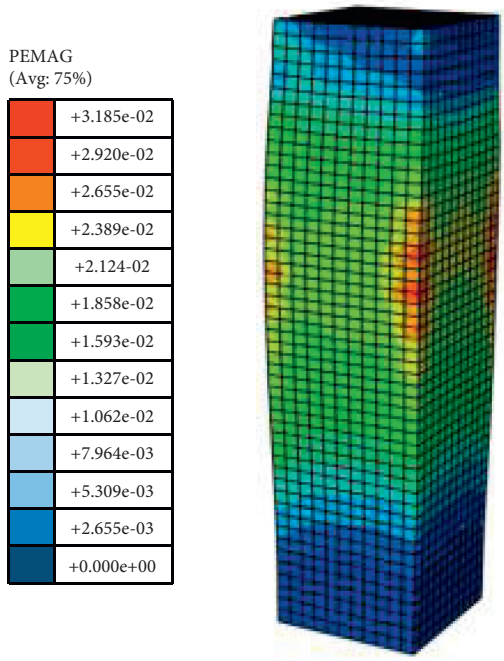

Figure 13: Strain cloud picture of RC3 (MPa).

6. Conclusions

The axial compression load-bearing capacity and mechanical properties of short concrete columns reinforced with prestressed angle steel plates were studied with the axial compression test of 20 specimen columns. Conclusions were drawn as follows:

(1) Compared with the control columns, the ultimate load-bearing capacity of each group of the reinforced columns was significantly increased (RC3 > RC2 > RC0 > CC). With the unidirectional compression, as the steel plate's prestress increased, the duration of the elastic stage was increased, indicating an increase in the stiffness. When the ultimate load was reached, the curve of load versus displacement declined more gently for the specimen with a greater prestress, showing increased ductility with an increase in the prestress.

(2) The curve of load versus strain of the reinforcement steel bar showed that a greater prestress resulted in an increase in the peak strain of the concrete in the elastic stage, that is, the strain corresponding to the ultimate load. However, a greater prestress also led to a greater deformation of the concrete, indicating that the prestressed angle steel plate could not effectively constrain the deformation of the concrete column.

(3) The test results were compared with the calculation results given by Equation (25). The comparison validated the good accuracy of the formula for the proposed new structure. The formula could provide design guidance for the calculation of the load-bearing capacity of the reinforced concrete columns.

(4) The finite element simulation accurately reflected the stress conditions of the concrete columns. The failure characteristics of the concrete columns simulated by the finite element model were in good agreement with the test results.

Data Availability

The data used to support the findings of this study are all included within the article.

Disclosure

The patent number is ZL201610919619.1.

Conflicts of Interest

The authors declare that they have no conflicts of interest.

Authors' Contributions

Conceptualization was done by Z. R. and X. Z.; methodology was developed by Z. R.; software was provided by Q. S.; validation was performed by X. Z.; formal analysis was performed by X. Z.; investigation was performed by Z. R. and X. Z.; resources was provided by Z. R. and X. Z.; data curation was performed by Q. S.; original draft was written by X. Z.; reviewing and editing were done by X. Z. and H. H.; visualization was performed by Z. R.; supervision was done by X. Z.; project administration was done by Z. R. and X. Z.; funding acquisition was done by Z. R. and X. Z. All authors have read and agreed to the published version of the manuscript.

Acknowledgments

This research was funded by the Fundamental Research Funds for the Key Project of Research and Development Plan of Hunan Province (2020SK2109) and National Natural Science Foundation of Hunan Province (2021JJ50106). The project was supported by Hunan Key Laboratory of Intelligent Disaster Prevention and Mitigation and Ecological Restoration in Civil Engineering, Catastrophe and Reinforcement of Dangerous Engineering Structures, Hunan Provincial Engineering Research Center.

References

[1] Z. H. Ren, X. T. Zeng, W. J. Qu, and Q. Liang, "Analysis of axial compression bearing capacity of rectangular concrete short columns strengthened with prestressed angle steel plate," *Building Structure*, vol. 48, no. 14, pp. 84–89+93, 2018.

[2] S. H. Cai, *Modern Steel Tube Confined Concrete Structures*, pp. 3–7, China Communications Press, Beijing, China, 2003.

[3] B. L. Liang and J. X. Liu, "Ultimate bearing capacity of concrete-filled circular steel tubular short columns under axial compression," *Journal og Shanghai Jiaotong University*, vol. 44, no. 6, pp. 749–753, 2010.

[4] Y. Qin, P. T. Wu, L. Huang, and Y. Lv, "Experimental study on the short columns of steel tube ultra-high performance concrete under axial compression," *Journal of Tianjin Chengjian University*, vol. 26, no. 04, pp. 254–259, 2020.

[5] J. S. Han, D. Yuli, Z. D. Xu, S. P. Cong, and W. R. Cheng, "Analysis of axial compression performance for reinforcement concrete-filled tubular steel," *Journal of civil, architectural &environmental engineering*, vol. 31, no. 03, pp. 11–17, 2009.

[6] Y. Y. Lu, H. Liang, S. Li, and X. Yin, "Experimental study on behavior of square RC columns strengthened with self-compacting concrete filled square steel tubes under axial load," *Journal of Building Structures*, vol. 36, no. 07, pp. 43–50, 2015.

[7] C. Y. Gao, Y. X. Duan, H. Zhang, and H. G. Yang, "Experimental study on the bearing capacity of circular tubed reinforced concrete short column under axial compression," *Building Structure*, vol. 47, no. 2, pp. 48–52, 2017.

[8] X. Hu, *Research on Compressive Performance and Bearing Capacity of RC Short Columns Strengthened with Circular Steel Jacketing*, Southwest Jiaotong University, Chengdu, China, 2014.

[9] J. Gao, *Performance Investigation of FRP Strengthened Reinforced concrete Circular Columns under Axial Compressive Loading*, Zhengzhou University, Zhengzhou, China, 2014.

[10] S. P. Yin, C. Peng, and S. X. Ai, "Research on the axial compression properties of concrete columns strengthened with textile reinforced concrete," *Journal of Sichuan University (Engineering Science Edition)*, vol. 48, no. 4, pp. 85–95, 2016.

[11] Y. Y. Lu, J. Y. Shi, and G. F. Zhao, "Experimental research on concrete columns strengthened with the combination of CFRP and angle steel," *Journal of Building Structures*, vol. 24, no. 5, pp. 18–23, 2003.

[12] L. Zeng, L. Li, J. Chen, X. Yang, and S. Peng, "Experimental study on concrete columns strengthened with non-adhesive carbon fibre spirals under axial compression," *Journal of Building Structures*, vol. 37, no. 5, pp. 283–290, 2016.

[13] Y. F. Ma, *Experimental Study on High-Strength concrete Restrained by CFRP Sheet under Axial Loading*, Hebei United University, Tangshan, China, 2014.

[14] L. J. Hao, *Research on Axial Compression Performance of concrete Column Strengthened by Prestressed Steel belt Reinforced*, Xi'an University of Architecture and Technology, Xi'an, China, 2014.

[15] Y. Zhao, *The Experimental Study on Axial Compression Performance of concrete Square Columns Strengthened with Prestressed Steel Strip*, Xi'an University of Architecture and Technology, Xi'an, China, 2014.

[16] B. Zhang, Y. Yang, Y. Liu, and L. J. Hao, "Experimental study on axial compression performance of reinforced concrete column retrofitted by prestressed steel strip," *Journal of Engineering Mechanics*, vol. 33, no. 3, pp. 104–111, 2016.

[17] L. Zhang, G. R. Ning, J. H. Li, and Y. Yang, "Experimental study of reinforced concrete columns strengthened by prestressed steel strips," *Industrial Construction*, vol. 46, no. 3, pp. 155–159, 2016.

[18] GB/T 50081-2002, *Standard for Test Method of Mechanical Properties on Ordinary concrete, Ministry of Construction PRC,General Administration of Quality Supervision*, Quarantine and Inspection, Beijing, China, 2002.

[19] P. Shen, *Design Theory for Concrete Structure*, Higher Education Press, Beijing, 4th edition, 2012.

[20] Y. U. Mao-hong, *Unified Strength Theory and Its Applications*, Springer Press, Berlin, 2004.

[21] Z. H. Guo and X. D. Shi, *Reinforced Concrete Theory and Analysis*, Tsinghua University Press, Beijing, 2003.

[22] Z. L. Xu, *Elasticity*, Vol. I, Higher Education Press, , Beijing, 2006.

[23] Z. Q. Zhang, J. H. Zhao, Y. F. Zhang, and X. W. Li, "Axial bearing capacity of composite concrete-filled steel tubular columns," *Journal of Chang'an University (Natural Science Edition)*, vol. 30, no. 1, pp. 67–70, 2010.

[24] J. H. Zhao and . Meng, "Bearing capacity of concrete-filled double-skin steel-tube stub column," *Journal of Chang'an University (Natural Science Edition)*, vol. 29, no. 1, pp. 70–74, 2009.

[25] Y. Zhai, J. H. Zhao, L. Ji, and X. Y. Wei, "Unified Solutions on axial compressive strength of concrete filled steel tube," *Journal of Chang'an University (Natural Science Edition)*, vol. 26, no. 3, pp. 55–58, 2006.

[26] J. H. Zhao, *Strength Theory and Engineering Application*, Science Press, Beijing, 2003.

[27] S. Wang, X. Jiang, and Y. Bai, "Nonlinear finite element analysis of axially loaded concrete-filled steel tubular stub columns," *Sciencepaper Online*, vol. 4, no. 07, pp. 472–479, 2009.